Hydrol. Earth Syst. Sci. Discuss., 12, 12483–12514, 2015
www.hydrol-earth-syst-sci-discuss.net/12/12483/2015/
doi:10.5194/hessd-12-12483-2015

Hydrology and Earth System Sciences Discussions

Open Access

An ice core derived 1013-year catchment scale annual rainfall reconstruction in subtropical eastern Australia

C. R. Tozer[1,2], T. R. Vance[1], J. Roberts[1,3], A. S. Kiem[2], M. A. J. Curran[1,3], and A. D. Moy[1,3]

[1]Antarctic Climate & Ecosystems Cooperative Research Centre, University of Tasmania, Hobart, Tasmania 7001, Australia
[2]Centre for Water, Climate and Land Use, University of Newcastle, Callaghan, NSW 2308, Australia
[3]Australian Antarctic Division, Kingston, Tasmania 7050, Australia

Received: 23 October 2015 – Accepted: 23 November 2015 – Published: 3 December 2015

Correspondence to: C. R. Tozer (carly.tozer@utas.edu.au)

Published by Copernicus Publications on behalf of the European Geosciences Union.

Abstract

Paleoclimate research indicates that the instrumental climate record (∼100 years in Australia) does not cover the full range of hydroclimatic variability possible. To better understand the implications of this for catchment-scale water resources management, an annual rainfall reconstruction is produced for the Williams River catchment in coastal eastern Australia. No high resolution palaeoclimate proxies are located in the region and so a teleconnection between summer sea salt deposition recorded in ice cores from East Antarctica and rainfall variability in eastern Australia was exploited to reconstruct 1013 years of rainfall (AD 1000–2012). The reconstruction shows that significantly longer and more frequent wet and dry periods were experienced in the preinstrumental compared to the instrumental period. This suggests that existing drought and flood risk assessments underestimate the true risks due to the reliance on data and statistics obtained from only the instrumental record. This raises questions about the robustness of existing water security and flood protection measures and has serious implications for water resources management, infrastructure design, and catchment planning. The method used in this proof of concept study is transferable and enables similar insights into the true risk of flood/drought to be gained for other locations that are teleconnected to East Antarctica. This will lead to improved understanding and ability to deal with the impacts of multidecadal to centennial hydroclimatic variability.

1 Introduction

Water and catchment management systems (e.g. drought and flood plans) and water resources infrastructure have traditionally been designed based on the trends, patterns and statistics revealed in relatively short instrumental climate records (i.e. for Australia usually less than 100 years of data recorded post-1900) (Razavi et al., 2015; Verdon-Kidd and Kiem, 2010; Ho et al., 2014; Cosgrove and Loucks, 2015). This is a concern as paleoclimate research suggests that instrumental climate records are not representative of the true range of hydroclimatic variability possible (Vance et al., 2015; Razavi et al., 2015; Ho et al., 2014, 2015a, b; Verdon-Kidd and Kiem, 2010; Gallant and Gergis, 2011; Kiem and Verdon-Kidd, 2011). For example, paleoclimate archives show evidence of droughts of longer duration than the three major droughts to affect eastern Australia over the instrumental period – Federation drought (∼ 1895–1902), World War II drought (∼ 1937–1945) and Millennium or "Big Dry" drought (∼ 1997 to 2009) (Vance et al., 2013, 2015; Gergis et al., 2012; Allen et al., 2015).

Sources for paleoclimate proxy data include tree rings, coral skeletons, ice cores, speleothems (cave deposits), sediments or documentary evidence (Ho et al., 2014). Ideally, the climate proxy archives are located in the region of interest (e.g. Cullen and Grierson, 2009; Oster et al., 2015; Sheppard et al., 2004; Allen et al., 2015). In areas where proxy records are sparse or of low resolution, remote proxies are a viable alternative (Ho et al., 2014). Remote proxies exploit circulation teleconnections that link one region to another and are calibrated over the instrumental period, to develop paleoclimate reconstructions (e.g. rainfall, streamflow) for the target region (e.g. Vance et al., 2013, 2015; van Ommen and Morgan, 2010; McGowan et al., 2009; Verdon and Franks, 2007). In this case the assumption is that large-scale climate processes driving climate variability at the location of the paleoclimate proxy also drive a high proportion of climate variability at the region of interest, assuming long term stationarity (Gallant and Gergis, 2011). For example, van Ommen and Morgan (2010) identified a relationship between precipitation (snowfall) recorded in ice cores from coastal Antarctica and rainfall in southwest Western Australia over the instrumental period, inferring rainfall variability in the region for the past 750 years. Similarly, Lough (2011) found significant correlations between coral luminescence intensity recorded in coral cores from the Great Barrier Reef and summer rainfall variability in northeast Queensland. The multicentury coral record could then be used to reconstruct Queensland summer rainfall back to the 18th century.

Another option is to use the link between large-scale ocean-atmospheric climate processes and climate variability in the region of interest to develop a paleoclimate

HESSD
12, 12483–12514, 2015

reconstruction based on a paleoclimate proxy of the climate process. For example, McGowan et al. (2009) used the previously identified relationship between sea surface temperature (SST) anomalies in the Pacific Ocean, in this case represented by the Pacific Decadal Oscillation (PDO), and streamflow in south-eastern Australia (e.g. Verdon et al., 2004; Kiem and Franks, 2004; Power et al., 1999a, b; Kiem et al., 2003) to produce a reconstruction of annual inflows in the Murray River back to AD 1474. A similar approach was also followed by Verdon and Franks (2007, 2006) and Henley et al. (2011).

Vance et al. (2013, 2015) used somewhat of a hybrid approach to those discussed above. Vance et al. (2013) developed a millennial length rainfall reconstruction for subtropical eastern Australia by exploiting a relationship between the region's annual rainfall and the sea salt record (see Sect. 3) from the Law Dome ice core, East Antarctica (Fig. 1). Of key importance, however, is that the relationship during the instrumental period (in this case 1889–2009) was found to vary synchronously with the Interdecadal Pacific Oscillation (IPO) (Power et al., 1999a, 1999b), the basin-wide expression of the PDO, with increased correlations found during IPO positive phases (Vance et al., 2013, 2015). The IPO represents decadal SST variability across the Pacific Ocean whereby a positive IPO phase is associated with warming across the tropical Pacific and cooling of the north and south Pacific; the opposite occurs during the negative phase (Power et al., 1999a). The most recent defined complete IPO phases are two positive phases (~ 1924–1941, ~ 1979–1997) and one negative phase (~ 1947–1975) (Power et al., 1999a; Verdon et al., 2004; Kiem and Franks, 2004; Kiem et al., 2003).

Vance et al. (2015) demonstrated that during the IPO negative phase there is a predominantly zonal pressure pattern across the high- to mid-latitudes which switches to a more meridional pattern in IPO positive. Folland et al. (2002) also found that during the IPO positive phase, the mean position of the South Pacific Convergence Zone (SPCZ) (usually bounded by Samoa and Fiji) is displaced northeast. This northeast displacement is associated with a more meridional circulation pattern and enhances the link between eastern Australia and mid- to high-latitude climate variability and hence

HESSD
12, 12483–12514, 2015

explains the stronger relationship between sea salt recorded at Law Dome and rainfall in eastern Australia during the IPO positive phase. Based on their reconstruction of the IPO, Vance et al. (2015) could therefore identify periods in time (i.e. positive IPO phases) where they had greater confidence in the rainfall reconstruction. A key finding from Vance et al. (2015) was the identification of a century of IPO positive aridity (AD 1102–1212), including evidence of a 39 year drought in southeast Queensland, which is well outside the bounds of instrumental drought duration. This illustrates the importance of investigating climate variability over millennial time-scales, particularly in the Southern Hemisphere where many paleoclimate records only span the last two hundred to five hundred years (Neukom and Gergis, 2012). Indeed, it is evident that: (a) instrumental data are not long enough to allow for meaningful planning for climate variability; (b) paleodata, particularly at the millennial time-scale, offers an important insight into the climate beyond the instrumental period; and (c) there is a need to incorporate insights from paleodata into water resources planning and management.

Further work is also required to assess the robustness of the relationship between climate variability in East Antarctica, large-scale climate processes and eastern Australia, a region with limited local paleoclimate proxy data (Vance et al., 2013; Ho et al., 2014). Practical usefulness of the insights provided by the paleoclimate reconstructions for water resources management at the catchment scale also requires investigation. Therefore, the links between the Law Dome sea salt record, eastern Australian rainfall and the IPO are further explored in this paper through the development of a millennial length, annual resolution, catchment-scale rainfall reconstruction for the Williams River (WR) catchment (Fig. 1). The WR catchment is located on the eastern seaboard of New South Wales, east of the Great Dividing Range (Fig. 1). The eastern seaboard contains about half of Australia's population, and a proportionate amount of economic infrastructure and activity. The region has hydroclimate features that are distinct from the rest of Australia (e.g. Verdon and Franks, 2005; Timbal, 2010) and no local, high resolution paleoclimate proxies (Ho et al., 2014). This means there is significant vulnerability, uncertainty and knowl-

HESSD
12, 12483–12514, 2015

edge gaps relating to flood and drought risk in eastern Australia. This recognition has recently motivated the development of the Eastern Seaboard Climate Change Initiative (ESCCI). ESCCI is a government funded initiative to better understand the causes and impacts of current and future climate related risk in eastern Australia (http://www.climatechange.environment.nsw.gov.au/About-climate-change-in-NSW/Evidence-of-climate-change/Eastern-seaboard-climate-change-initiative). The WR catchment is of particular regional importance because it forms part of the conjunctive-use headworks scheme for potable water supply to ~ 600 000 people in Newcastle, the sixth largest residential region in Australia (Kiem and Franks, 2004; Mortazavi-Naeini et al., 2015).

In the following sections we present a description of the WR catchment location and relevant climate data, including a discussion of the link between Law Dome, East Antarctica and eastern Australia. We proceed with an investigation into the relationship between summer sea salts from Law Dome and rainfall in the WR catchment and follow with the development of a 1013 year catchment-scale rainfall reconstruction for the WR (based on the Law Dome sea salt record) and discussion of the insights and implications emerging from this rainfall reconstruction.

2 Rainfall variability in the Williams River catchment

For this study we used daily 5 km ×5 km gridded rainfall data obtained from the Australian Water Availability Project (AWAP) (Jones et al., 2009) for the period 1900–2010. The AWAP grids overlapping the WR catchment were extracted and used to calculate catchment average monthly rainfall totals for the WR catchment. Due to known biases and uncertainty associated with gridded climate data (e.g. Tozer et al., 2012), the AWAP-based information was ground-truthed with data from a high quality (Lavery et al., 1997) rainfall gauge (61010) located within the WR catchment. Figure 2 shows the mean and standard deviation of monthly rainfall recorded at the 61010 gauge and for the AWAP catchment average. The highest and most variable rainfall in the WR

HESSD
12, 12483–12514, 2015

catchment is received from December to May (summer and autumn) and the hydrological water year for the WR catchment is therefore defined as October to September in order to encompass this high rainfall period (B. Berghout, Senior Water Resources Engineer, Hunter Water Commission, personal communication, 2015).

Rainfall variability in the WR catchment is associated with several large-scale ocean-atmospheric processes (e.g. Kiem and Franks, 2001, 2004; Risbey et al., 2009). The El Niño Southern Oscillation (ENSO) and IPO have been related to interannual to multidecadal variability in both WR rainfall and runoff (Kiem and Franks, 2001, 2004). Drier (wetter) catchment conditions typically occur during El Niño (La Niña) events and the IPO modulates both the frequency and magnitude of ENSO impacts such that drought risk is increased during IPO positive phases and flood risk is increased during IPO negative phases (Kiem and Franks, 2001, 2004; Kiem et al., 2003; Kiem and Verdon-Kidd, 2013). Climate mechanisms stemming from the Indian Ocean (Gallant et al., 2012; Verdon and Franks, 2005) and mid- to high-latitudes (e.g. blocking Risbey et al., 2009), the Subtropical Ridge (e.g. Whan et al., 2013; Timbal and Drosdowsky, 2013) and the Southern Annular Mode (SAM) (e.g. Meneghini et al., 2007; Ho et al., 2012), have also been found to be associated with hydroclimatic variability in the study region. In addition, the WR catchment is subject to synoptic scale influences known as East Coast Lows (ECLs), marine or continental low pressure systems that are responsible for much of the extreme weather (e.g. heavy rainfall, high winds) recorded in eastern New South Wales (Speer et al., 2009; Pepler et al., 2014; Ji et al., 2015; Browning and Goodwin, 2013; Kiem et al., 2015; Twomey and Kiem, 2015a, b).

3 The Law Dome-eastern Australia rainfall proxy

3.1 Law Dome ice core site details

Law Dome is a small, coastal icecap located in Wilkes Land, East Antarctica (Fig. 1). The primary ice core site, “Dome Summit South” (DSS) is located at 66°46′11″ S, 112°48′25″ E, elevation 1370 m, 4.7 km SSW of the summit (Morgan et al., 1997). The main DSS core was drilled in 1987–1993 and is 1370 m long spanning 90 000 plus years (Roberts et al., 2015). DSS has high annual snowfall of around 0.63 m (water equivalent). This high snowfall allows for the sampling of the seasonal variation in snow chemistry in the upper of the core and hence highly accurate dating (Roberts et al., 2015; Vance et al., 2013).

The Law Dome summer (December–March) sea salt (LD_{SSS}) record was developed from a 2000 year volcanic dating study from the Law Dome ice core (Plummer et al., 2012). Plummer et al. (2012) used independent annual layer-counting to date the record and known volcanic horizons to establish dating accuracy. As a result, the Law Dome record was dated with absolute accuracy from AD 1807–2009 and with ±1 year error from AD 894–1807. The sea salt record used here was produced via trace ion chromatography from 2.5–5 cm sub-samples of the ice cores (Curran et al., 1998; Palmer et al., 2001). Here we extend the 1010 year LD_{SSS} record of Vance et al. (2013, 2015) to cover the epoch AD 1000–2012 by using the improved composite record of Roberts et al. (2015).

3.2 The link between sea salt deposition at Law Dome and large-scale ocean–atmospheric processes

The climate signals recorded in the Law Dome ice core are driven by large-scale ocean–atmospheric processes rather than local factors (Delmotte et al., 2000; Masson-Delmotte et al., 2003; Vance et al., 2013; Bromwich, 1988). The southern Indian Ocean is the main source of moisture delivered to Law Dome (Delmotte et al., 2000; Masson-Delmotte et al., 2003) and sea salt deposition is related to the mid-latitude westerly winds (associated with the SAM) in the Indian and Pacific sectors of the Southern Ocean (Goodwin et al., 2004; Vance et al., 2015). It is thought that the SST anomalies in the central-western equatorial Pacific associated with ENSO propagate to high southern latitudes via Rossby wave activity (Karoly, 1989). The resulting circumpolar geopotential height and zonal wind anomalies influence the SAM (L'Heureux and

Thompson, 2006), and ultimately deliver sea salt aerosols to coastal Antarctica (Vance et al., 2013). Indeed, Vance et al. (2013) found a significant correlation between ENSO-related SST variability in the central-western equatorial Pacific and LD_{SSS}, with low summer sea salt years associated with El Niño events over the period 1889–2009. Furthermore, spectral analysis of the 1010 year LD_{SSS} record found significant ($p < 0.01$) spectral features in the 2–7 year ENSO band. Similar to the LD_{SSS} rainfall proxy discussed previously, the LD_{SSS} ENSO proxy varies decadally, coherent with the IPO, with a stronger relationship during IPO positive phases (Vance et al., 2013, 2015).

It is thus clear that the ocean–atmospheric processes associated with sea salt deposition at Law Dome (e.g. IPO, ENSO, SAM and variability in Indian Ocean SSTs) also influence rainfall variability in the WR catchment (discussed in Sect. 2). We can therefore expect LD_{SSS} variability to explain some variability in the rainfall recorded in the WR catchment.

4 Investigating the relationship between LD_{SSS} and rainfall in the Williams River catchment

Vance et al. (2013) found a relationship between LD_{SSS} and the prior January–December rainfall west of the Great Dividing Range (see Fig. 1). As the region of interest in this study is further south and east of the Great Dividing Range we needed to re-evaluate if this temporal offset was appropriate. To do this, for every AWAP grid-cell in New South Wales we performed linear least squares regression (using the Marquardt-Levenberg method) between the LD_{SSS} record and 12 month averaged rainfall over a 24 month lead/lag window centred about the summer sea salt period (December–March). The regression coefficients for each lead/lag were used to generate an estimated rainfall time-series for each grid-cell. The Pearson correlation between the estimated rainfall and AWAP rainfall for each grid-cell was then assessed for each lead/lag.

From the lead/lag analysis October–September and November–October annual rainfall in the region encompassing the WR catchment was found to have the highest and most spatially coherent relationship with LD_{SSS}. We present the October–September rainfall/LD_{SSS} correlations (Fig. 3) as this period also corresponds to the water year in the Newcastle region (discussed in Sect. 2) and hence all further analysis is based on the 12 month rainfall totals calculated from October–September.

Figure 3 shows the magnitude of the correlations between October–September WR rainfall and LD_{SSS} for the 1900–2010 (i.e. October 1900–September 2010) period as well as subsets for the different IPO phases. For comparison Fig. 3a–e are inset with maps for the January–December rainfall/LD_{SSS} correlations, the analysis period used in Vance et al. (2013, 2015). Figure 3f indicates the 13 year moving window correlations between LD_{SSS} and October–September for rainfall recorded at gauge 61010 and the AWAP WR catchment average, to identify low frequency variability associated with the IPO (Vance et al., 2015). The Pearson correlations with bootstrap confidence intervals (Mudelsee, 2003) between LD_{SSS} and October–September annual rainfall recorded at gauge 61010 and the AWAP WR catchment average for the full record and IPO phases are presented in Table 1.

The insets of Fig. 3a–e reveal low correlations in the WR catchment region. The highest correlations occur in inland New South Wales and into southeast Queensland, the focus region of Vance et al. (2013, 2015). However, when the correlation is aligned with the WR catchment water year (October–September) we see a shift in the region of significant correlation (Fig. 3a) to coastal New South Wales and in particular, large parts of the eastern seaboard. Importantly, correlations significant at the 99 % level are seen over the WR catchment region. Rainfall at gauge 61010 and AWAP catchment average show significant correlations with LD_{SSS} (Pearson correlation values of 0.29 and 0.28 respectively) over the 1900–2010 period (Table 1).

As expected, based on the results of Vance et al. (2013, 2015) (discussed in Sect. 3), the strength of the correlation between October–September rainfall and LD_{SSS} varies decadally. Figure 3b and c indicates that the relationship between the variables is stronger during the IPO positive phases relative to the negative phase. Figure 3d and e and the results in Table 1, however, suggest that although the relationship between

October–September rainfall and LD_{SSS} is stronger in IPO positive phase, this increase in strength relative to IPO negative and the full record (1900–2010) is primarily due to the very high correlation in the second IPO positive phase (1979–1997). In fact, the correlation between rainfall recorded at gauge 61010 and LD_{SSS} during the IPO negative phase is greater than the correlation in the first IPO positive phase (Table 1).

On the surface this result appears to be in contrast to Vance et al. (2013, 2015) who found a clear link between IPO phase and LD_{SSS}/January–December rainfall in southeast Queensland and northeast New South Wales (west of the Great Dividing Range). That is, the correlation between these variables was near zero during the whole IPO negative phase, yet was significant for both IPO positive phases. A key difference between this study and Vance et al. (2013, 2015) is that the focus region is further south, on the coast and under the orographic influence of the Great Dividing Range. Although interdecadal and interannual tropical Pacific Ocean variability (e.g. ENSO and IPO) has been found to impact the whole of Australia at various times of the year (e.g. Risbey et al., 2009; Power et al., 1999a), the amount of rainfall variability explained by these processes reduces the further south the region of interest is located (Risbey et al., 2009) and climate mechanisms stemming from the mid- to high-latitudes (e.g. Whan et al., 2013; Timbal and Drosdowsky, 2013; Meneghini et al., 2007; Ho et al., 2012; Kiem and Verdon-Kidd, 2010, 2009) increase their influence on rainfall variability.

As mentioned, the eastern seaboard is also subject to synoptic scale intense weather systems like ECLs. In 1950 and 1955 the Newcastle region experienced severe ECLs that resulted in heavy rainfall and severe floods (Callaghan and Helman, 2008; Callaghan and Power, 2011, 2014). The relationship between LD_{SSS} and rainfall in the WR catchment could not be expected to hold during these short duration but intense local-scale weather events. As such, this period of elevated ECL activity (e.g. Browning and Goodwin, 2015) largely explains the marked reduction (and change of sign) in the correlation between LD_{SSS} and rainfall in the WR catchment in the early 1950s (Fig. 3f). ECL variability has been related to the IPO, with Speer (2008) finding that during the

HESSD
12, 12483–12514, 2015

An ice core derived 1013-year catchment scale annual rainfall reconstruction

C. R. Tozer et al.

second IPO positive phase (i.e. 1979–1997) there was a decrease in ECLs relative to IPO negative. This would correspond to a reduction in ECL-related rainfall over New South Wales in the most recent IPO positive phase and is further evidence that ECLs affect the relationship between LD_{SSS} and rainfall in the WR catchment. While a better understanding of the role of ECLs (and other synoptic scale weather processes) may improve our understanding of the variability in the strength of the LD_{SSS} and WR rainfall teleconnection (particularly in the IPO negative phases which appear to favour increased ECL activity and "storminess", Callaghan and Helman, 2008; Callaghan and Power, 2011; Kiem and Verdon-Kidd, 2013; Browning and Goodwin, 2015), the relationship between LD_{SSS} and WR rainfall is significant and hence LD_{SSS} variability can be used to provide insights into preinstrumental rainfall variability in the WR catchment (see Sect. 5).

5 Reconstructing rainfall in the Williams River catchment

5.1 Development of the Williams River rainfall reconstruction

The linear regression coefficients determined for the instrumental calibration period (Sect. 4) were applied to the AD 1000–2012 LD_{SSS} data to produce 1013 years of rainfall data for each AWAP grid-cell in the WR catchment. This grid-cell data was then spatially averaged to produce a WR catchment average rainfall reconstruction time-series.

5.2 Comparing the catchment average rainfall reconstruction with instrumental (AWAP) data

A comparison between the AWAP catchment average and reconstructed WR catchment rainfall over the instrumental period (1900–2010) is presented in Fig. 4. The pattern of peaks and troughs in the recorded rainfall is well represented in the reconstruction but the range of variability is underestimated. The rainfall reconstruction captures

HESSD
12, 12483–12514, 2015

around 10 % of the rainfall variability in the WR catchment (Table 1). Nonetheless, as discussed above, there are periods when a stronger relationship between LD_{SSS} and rainfall in the WR catchment exist. For example, during the second IPO positive phase (1979–1997) the rainfall reconstruction captures around 40 % of the WR rainfall variability (Table 1). Where peaks and troughs do not match, it may be related to the occurrence of short duration intense weather events such as the ECLs in the 1950s mentioned previously.

Ultimately, while no paleoclimate proxy will ever be perfect, Figs. 3 and 4 and Table 1 show that the LD_{SSS} based rainfall reconstruction provides a useful indication of rainfall in the WR catchment over the instrumental period and hence can be used to gain insights into preinstrumental rainfall variability in the WR region.

5.3 A millennial rainfall reconstruction for the WR catchment

Figure 5 presents the 1013 year rainfall reconstruction produced for the WR catchment. Encouragingly, periods post-1900 that are known to be associated with droughts and flooding in the WR catchment are identified in the reconstruction (e.g. the World War II) drought in the late 1930s, the Millennium drought in the 1990s to 2000s, and the flood dominated 1950s (e.g. Callaghan and Power, 2014; Verdon-Kidd and Kiem, 2009; Gallant et al., 2012). From the 10 year smoothed record it is evident that there have been multi-year periods of either above or below average rainfall. A multi-century dry period is evident from around AD 1100–1250 while two similarly persistent wet periods are seen from around AD 1400–1600 and 1800–1900. The early dry period overlaps with a sustained warm period generally referred to as the Medieval Warm Period (∼ AD 950–1250). Though there is little published evidence that this period was a feature of the Australasian climate (Reeves et al., 2013), it appears to be a feature of a recently published Southern Hemisphere reconstruction (Neukom et al., 2014).

In the context of the last 1000 years, Fig. 5 shows that the recent era (1900–present) is relatively dry and less variable. The 10 year moving average rarely exceeds the long term 1013 year average, even in the 1950–1970 period which was associated with

HESSD
12, 12483–12514, 2015

multiple significant flood events across eastern Australia (Kiem et al., 2003; Kiem and Verdon-Kidd, 2013; Callaghan and Power, 2014). While not in the same region as the WR catchment, other nearby shorter proxy records also suggest that the 20 century has been relatively dry (Gallant and Gergis, 2011; Gergis et al., 2012).

While Fig. 5 gives insights into periods of above and below average rainfall, of particular interest for hydrological studies and water resources management is not just whether a year or sequence of years is above or below the long term average but whether a multiyear or multidecadal epoch is generally wet or dry even though some years within that epoch may be slightly below or above the long term average. For example, a year that is only 0.1 standard deviations above the average probably will not provide enough rainfall to break a drought or fill reservoirs. To account for this we define "wet" and "dry" years as Eq. 1:

$$\begin{aligned} \text{wet} &= \text{years where rainfall} > \text{mean} - x \times \text{standard deviation} \\ \text{dry} &= \text{years where rainfall} < \text{mean} + x \times \text{standard deviation} \end{aligned} \tag{1}$$

Table 2 compares the persistence of the longest above and below average rainfall periods ($x = 0$ in Eq. 1), and "wet/dry" periods, in the AWAP catchment average rainfall and the reconstruction. As shown in Table 2 (rows 2 and 3) the reconstruction captures the dry periods, in terms of duration and timing, of the AWAP instrumental record well and also the duration of the longest wet periods. However, the timing of the wettest periods detected by the reconstruction is different to that seen in the AWAP record. As previously discussed this is likely due to the inability of the LD_{SSS} reconstruction to characterise local-scale synoptic activity in the WR region (i.e. ECLs). Importantly, this also implies that the wettest epochs in the reconstruction may be an underestimation, as the reconstruction is least accurate during wet periods caused predominantly by local-scale influences (e.g. ECLs). In other words, wet periods associated with increased ECL activity (e.g. similar to the 1950s) are possible and the magnitude of rainfall associated with these events would be over and above the preinstrumental wet epochs suggested by the LD_{SSS} reconstruction.

HESSD
12, 12483–12514, 2015

Figure 6 shows the duration of above and below average rainfall periods during each century since AD 1000 (and also for the whole 1013 year reconstruction period). To easily visualise the results, Fig. 6 combines all durations > 15 years (information on all durations is included Table S1 in the Supplement). Figure 6 clearly shows that (a) some centuries are drier (more pink) than others (more blue) and (b) the most recent complete century (1900–1999), where the majority of our instrumental record comes from, is not representative of either the duration or frequency of periods of above average rainfall experienced pre-1900.

While the results in Fig. 6 are important, of greater interest is the identification of persistent periods that were dry (or wet) overall even though some years within the otherwise dry (wet) regime were slightly wetter (drier) than average. Table 2 shows that using the threshold approach outlined in Eq. (1) does not noticeably change the duration of the longest wet or dry periods in the instrumental period. However, when dry and wet epochs (relative to the instrumental mean (1100.0 mm) and using a mid-range standard deviation threshold ($x = 0.3$)) are extracted from the preinstrumental reconstruction (Table 2, row 3) the longest dry epochs persist for up to 12 years instead of a maximum of 8 years post-1900 while wet epochs have lasted almost five times as long (maximum of 39 years preinstrumental compared to a maximum of 8 years in the instrumental period). Similar is seen if the long term (1000–2012) reconstruction mean (1126.1 mm) is used to indicate wet or dry (Table 2, row 3), with both the dry and wet epochs persisting up to twice as long preinstrumental as they have in the instrumental period. Figure 7 (and the associated Tables S2 and S3 in the Supplement) further illustrates this point (and the points made in relation to Fig. 6) by clearly showing that the proportion, magnitude, frequency or duration of wet/dry epochs in the instrumental period (1900–1999) is not representative of either the overall situation throughout the last 1000 years or the situation in any century pre-1900.

HESSD
12, 12483–12514, 2015

6 Conclusions

This study produced a 1013 year rainfall reconstruction for the WR catchment, a location without any local paleoclimate proxies. The strength of the relationship between LD_{SSS} and annual WR rainfall was found to vary decadally but, unlike Vance et al. (2013, 2015), was not always coherent with the IPO. Results suggest that this is due to the different climate regime that the coastal WR catchment is subject to compared to the previous studies which were located further north and predominantly west of the Great Dividing Range. The WR catchment is strongly influenced by local-scale coastal storms such as ECLs and this is the likely explanation for the different relationship to the IPO, as well as the breakdown in the East Antarctic-WR teleconnection in periods associated with increased ECL activity (e.g. the 1950s).

Despite this acknowledged limitation (which is being addressed in ongoing research) the relationship between LD_{SSS} and rainfall in the WR catchment is significant over the full instrumental calibration period. The LD_{SSS}-based reconstruction clearly shows that the instrumental period (~ 1900–2010) is not representative of the proportion, magnitude, frequency or duration of wet/dry epochs in any century in the preinstrumental era. This is consistent with recent independent studies focussed on Tasmania (Allen et al., 2015) and the Murray-Darling Basin (Ho et al., 2015a, b).

These findings provide compelling evidence to support the conclusion that existing hydroclimatic risk assessment and associated water resources management, infrastructure design, and catchment planning in the WR catchment is flawed given the reliance on drought and flood statistics derived from post-1900 information. Figure 3 (and Fig. 4a in Vance et al., 2015) suggests that the same is true for most of eastern Australia, and anywhere else with similar teleconnections with East Antarctica. Therefore, the robustness of existing flood and drought risk quantification and management in eastern Australia is questionable, especially given the multidecadal and centennial hydroclimatic variability demonstrated in this study.

HESSD
12, 12483–12514, 2015

The Supplement related to this article is available online at doi:10.5194/hessd-12-12483-2015-supplement.

Acknowledgements. This work was supported by the Australian Government's Cooperative Research Centres Programme through the Antarctic Climate and Ecosystems Cooperative Research Centre (ACE CRC). The Australian Antarctic Division provided funding and logistical support for the DSS ice cores (AAS projects 4061 and 4062). The Centre for Water, Climate and Land Use at the University of Newcastle provided partial funding for Tozer's salary.

References

Allen, K. J., Nichols, S. C., Evans, R., Cook, E. R., Allie, S., Carson, G., Ling, F., and Baker, P. J.: Preliminary December–January inflow and streamflow reconstructions from tree rings for western Tasmania, southeastern Australia, Water Resour. Res., 51, 5487–5503, doi:10.1002/2015WR017062, 2015.

Bromwich, D. H.: Snowfall in high southern latitudes, Rev. Geophys., 26, 149–168, doi:10.1029/RG026i001p00149, 1988.

Browning, S. A. and Goodwin, I. D.: Large-scale influences on the evolution of winter subtropical maritime cyclones affecting Australia's east coast, Mon. Weather Rev., 141, 2416–2431, doi:10.1175/MWR-D-12-00312.1, 2013.

Browning, S. A. and Goodwin, I. D.: Large scale drivers of Australian East Coast Cyclones since 1871, Austr. Meteorol. Oceanogr. J., AMOJ issue on the Eastern Seaboard Climate Change Initiative – East Coast Low (ESCCI-ECL) Program, in review, 2015.

Callaghan, J. and Helman, P.: Severe storms on the east coast of Australia 1770–2008, Griffith Centre for Coastal Management, Griffith University, Southport, Australia, 2008.

Callaghan, J. and Power, S.: Variability and decline in the number of severe tropical cyclones making land-fall over eastern Australia since the late nineteenth century, Clim. Dynam., 37, 647–662, doi:10.1007/s00382-010-0883-2, 2011.

Callaghan, J. and Power, S.: Major coastal flooding in southeastern Australia 1860–2012, associated deaths and weather systems, Austr. Meteorol. Oceanogr. J., 64, 183–213, 2014.

Cosgrove, W. J. and Loucks, D. P.: Water management: current and future challenges and research directions, Water Resour. Res., 51, 4823–4839, doi:10.1002/2014WR016869, 2015.

Cullen, L. and Grierson, P.: Multi-decadal scale variability in autumn-winter rainfall in south-western Australia since 1655 AD as reconstructed from tree rings of Callitris columellaris, Clim. Dynam., 33, 433–444, doi:10.1007/s00382-008-0457-8, 2009.
Curran, M. A. J., van Ommen, T. D., and Morgan, V.: Seasonal characteristics of the major ions in the high-accumulation Dome Summit South ice core, Law Dome, Antarctica, in: Annals of Glaciology, edited by: Budd, W. F., Int. Glaciological Soc., Cambridge, 27, 385–390, 1998.
Delmotte, M., Masson, V., Jouzel, J., and Morgan, V. I.: A seasonal deuterium excess signal at Law Dome, coastal eastern Antarctica: a southern ocean signature, J. Geophys. Res.-Atmos., 105, 7187–7197, doi:10.1029/1999JD901085, 2000.
Folland, C. K., Renwick, J. A., Salinger, M. J., and Mullan, A. B.: Relative influences of the Interdecadal Pacific Oscillation and ENSO on the South Pacific Convergence Zone, Geophys. Res. Lett., 29, 21-1–21-4, doi:10.1029/2001GL014201, 2002.
Gallant, A. J. E. and Gergis, J.: An experimental streamflow reconstruction for the River Murray, Australia, 1783–1988, Water Resour. Res., 47, W00G04, doi:10.1029/2010WR009832, 2011.
Gallant, A. J. E., Kiem, A. S., Verdon-Kidd, D. C., Stone, R. C., and Karoly, D. J.: Understanding hydroclimate processes in the Murray-Darling Basin for natural resources management, Hydrol. Earth Syst. Sci., 16, 2049–2068, doi:10.5194/hess-16-2049-2012, 2012.
Gergis, J., Gallant, A., Braganza, K., Karoly, D., Allen, K., Cullen, L., D'Arrigo, R., Goodwin, I., Grierson, P., and McGregor, S.: On the long-term context of the 1997–2009 "Big Dry" in South-Eastern Australia: insights from a 206-year multi-proxy rainfall reconstruction, Climatic Change, 111, 923–944, doi:10.1007/s10584-011-0263-x, 2012.
Goodwin, I. D., van Ommen, T. D., Curran, M. A. J., and Mayewski, P. A.: Mid latitude winter climate variability in the South Indian and southwest Pacific regions since 1300 AD, Clim. Dynam., 22, 783–794, doi:10.1007/s00382-004-0403-3, 2004.
Henley, B. J., Thyer, M. A., Kuczera, G., and Franks, S. W.: Climate-informed stochastic hydrological modeling: incorporating decadal-scale variability using paleo data, Water Resour. Res., 47, W11509, doi:10.1029/2010WR010034, 2011.
Ho, M., Kiem, A. S., and Verdon-Kidd, D. C.: The Southern Annular Mode: a comparison of indices, Hydrol. Earth Syst. Sci., 16, 967–982, doi:10.5194/hess-16-967-2012, 2012.
Ho, M., Verdon-Kidd, D. C., Kiem, A. S., and Drysdale, R. N.: Broadening the spatial applicability of paleoclimate information – a case study for the Murray–Darling Basin, Australia, J. Climate, 27, 2477–2495, doi:10.1175/JCLI-D-13-00071.1, 2014.

HESSD
12, 12483–12514, 2015

An ice core derived 1013-year catchment scale annual rainfall reconstruction

C. R. Tozer et al.

Ho, M., Kiem, A. S., and Verdon-Kidd, D. C.: A paleoclimate rainfall reconstruction in the Murray–Darling Basin (MDB), Australia: 1. Evaluation of different paleoclimate archives, rainfall networks, and reconstruction techniques, Water Resour. Res., 51, 8362–8379, doi:10.1002/2015WR017058, 2015a.

Ho, M., Kiem, A. S., and Verdon-Kidd, D. C.: A paleoclimate rainfall reconstruction in the Murray–Darling Basin (MDB), Australia: 2. Assessing hydroclimatic risk using paleoclimate records of wet and dry epochs, Water Resour. Res., 51, 8380–8396, doi:10.1002/2015WR017059, 2015b.

Ji, F., Evans, J., Argueso, D., Fita, L., and Di Luca, A.: Using large-scale diagnostic quantities to investigate change in East Coast Lows, Clim. Dynam., 45, 2443–2453, doi:10.1007/s00382-015-2481-9, 2015.

Jones, D. A., Wang, W., and Fawcett, R.: High-quality spatial climate data-sets for Australia, Austr. Meteorol. Oceanogr. J., 58, 233–248, 2009.

Karoly, D. J.: Southern Hemisphere circulation features associated with El Niño–Southern Oscillation Events, J. Climate, 2, 1239–1252, doi:10.1175/1520-0442(1989)002<1239:shcfaw>2.0.co;2, 1989.

Kiem, A. S. and Franks, S. W.: On the identification of ENSO-induced rainfall and runoff variability: a comparison of methods and indices, Hydrolog. Sci. J., 46, 1–13, 2001.

Kiem, A. S. and Franks, S. W.: Multi-decadal variability of drought risk, eastern Australia, Hydrol. Process., 18, 2039–2050, doi:10.1002/hyp.1460, 2004.

Kiem, A. S. and Verdon-Kidd, D. C.: Climatic drivers of Victorian Streamflow: is ENSO the dominant influence?, Austr. J. Water Resour., 13, 17–29, 2009.

Kiem, A. S. and Verdon-Kidd, D. C.: Towards understanding hydroclimatic change in Victoria, Australia – preliminary insights into the "Big Dry", Hydrol. Earth Syst. Sci., 14, 433–445, doi:10.5194/hess-14-433-2010, 2010.

Kiem, A. S. and Verdon-Kidd, D. C.: Steps toward "useful" hydroclimatic scenarios for water resource management in the Murray-Darling Basin, Water Resour. Res., 47, W00G06, doi:10.1029/2010WR009803, 2011.

Kiem, A. S. and Verdon-Kidd, D. C.: The importance of understanding drivers of hydroclimatic variability for robust flood risk planning in the coastal zone, Austr. J. Water Resour., 17, 126–134, 2013.

Kiem, A. S., Twomey, C., Lockart, N., Willgoose, G., Kuczera, G., Chowdhury, A. F. M. K., Parana Manage, N., and Zhang, L.: Links between East Coast Lows (ECLs) and the spatial and temporal variability of rainfall along the eastern seaboard of Australia (ESA), Austr. Meteorol. Oceanogr. J., AMOJ issue on the Eastern Seaboard Climate Change Initiative – East Coast Low (ESCCI-ECL) Program, in review, 2015.

L'Heureux, M. L. and Thompson, D. W. J.: Observed Relationships between the El Niño–Southern Oscillation and the Extratropical Zonal-Mean Circulation, J. Climate, 19, 276–287, doi:10.1175/JCLI3617.1, 2006.

Lavery, B., Joung, G., and Nicholls, N.: An extended high-quality historical rainfall dataset for Australia, Aust. Meteorol. Mag., 46, 27–38, 1997.

Lough, J. M.: Great Barrier Reef coral luminescence reveals rainfall variability over northeastern Australia since the 17th century, Paleoceanography, 26, PA2201, doi:10.1029/2010PA002050, 2011.

Masson-Delmotte, V., Delmotte, M., Morgan, V., Etheridge, D., van Ommen, T., Tartarin, S., and Hoffmann, G.: Recent southern Indian Ocean climate variability inferred from a Law Dome ice core: new insights for the interpretation of coastal Antarctic isotopic records, Clim. Dynam., 21, 153–166, doi:10.1007/s00382-003-0321-9, 2003.

McGowan, H. A., Marx, S. K., Denholm, J., Soderholm, J., and Kamber, B. S.: Reconstructing annual inflows to the headwater catchments of the Murray River, Australia, using the Pacific Decadal Oscillation, Geophys. Res. Lett., 36, L06707, doi:10.1029/2008GL037049, 2009.

Meneghini, B., Simmonds, I., and Smith, I. N.: Association between Australian rainfall and the Southern Annular Mode, Int. J. Climatol., 27, 109–121, doi:10.1002/joc.1370, 2007.

Morgan, V., Wookey, C. W., Li, J., Van Ommen, T., Skinner, W., and Fitzpatrick, M. F.: Site information and initial results from deep ice drilling on Law Dome, Antarctica, J. Glaciol., 43, 1–8, 1997.

Mortazavi-Naeini, M., Kuczera, G., Kiem, A. S., Cui, L., Henley, B., Berghout, B., and Turner, E.: Robust optimization to secure urban bulk water supply against extreme drought and uncertain climate change, Environ. Modell. Softw., 69, 437–451, doi:10.1016/j.envsoft.2015.02.021, 2015.

Mudelsee, M.: Estimating Pearson's correlation coefficient with bootstrap confidence interval from serially dependent time series, Math. Geol., 35, 651–665, doi:10.1023/B:MATG.0000002982.52104.02, 2003.

Neukom, R. and Gergis, J.: Southern Hemisphere high-resolution palaeoclimate records of the last 2000 years, Holocene, 22, 501–524, doi:10.1177/0959683611427335, 2012.

Neukom, R., Gergis, J., Karoly, D. J., Wanner, H., Curran, M., Elbert, J., Gonzalez-Rouco, F., Linsley, B. K., Moy, A. D., Mundo, I., Raible, C. C., Steig, E. J., van Ommen, T., Vance, T., Villalba, R., Zinke, J., and Frank, D.: Inter-hemispheric temperature variability over the past millennium, Nature Clim. Change, 4, 362–367, doi:10.1038/nclimate2174, http://www.nature.com/nclimate/journal/v4/n5/abs/nclimate2174.html#supplementary-information, 2014.

Oster, J. L., Montañez, I. P., Santare, L. R., Sharp, W. D., Wong, C., and Cooper, K. M.: Stalagmite records of hydroclimate in central California during termination 1, Quaternary Sci. Rev., 127, 199–214, doi:10.1016/j.quascirev.2015.07.027, 2015.

Palmer, A. S., van Ommen, T. D., Curran, M. A. J., Morgan, V., Souney, J. M., and Mayewski, P. A.: High-precision dating of volcanic events (AD 1301–1995) using ice cores from Law Dome, Antarctica, J. Geophys. Res.-Atmos., 106, 28089–28095, doi:10.1029/2001JD000330, 2001.

Pepler, A. S., Di Luca, A., Ji, F., Alexander, L. V., Evans, J. P., and Sherwood, S. C.: Impact of identification method on the inferred characteristics and variability of Australian East Coast Lows, Mon. Weather Rev., 143, 864–877, doi:10.1175/MWR-D-14-00188.1, 2014.

Plummer, C. T., Curran, M. A. J., van Ommen, T D., Rasmussen, S. O., Moy, A. D., Vance, T. R., Clausen, H. B., Vinther, B. M., and Mayewski, P. A.: An independently dated 2000 yr volcanic record from Law Dome, East Antarctica, including a new perspective on the dating of the 1450s CE eruption of Kuwae, Vanuatu, Clim. Past, 8, 1929–1940, doi:10.5194/cp-8-1929-2012, 2012.

Power, S., Casey, T., Folland, C., Colman, A., and Mehta, V.: Inter-decadal modulation of the impact of ENSO on Australia, Clim. Dynam., 15, 319–324, doi:10.1007/s003820050284, 1999a.

Power, S., Tseitkin, F., Mehta, V., Lavery, B., Torok, S., and Holbrook, N.: Decadal climate variability in Australia during the twentieth century, Int. J. Climatol., 19, 169–184, doi:10.1002/(sici)1097-0088(199902)19:2<169::aid-joc356>3.0.co;2-y, 1999b.

Razavi, S., Elshorbagy, A., Wheater, H., and Sauchyn, D.: Toward understanding nonstationarity in climate and hydrology through tree ring proxy records, Water Resour. Res.,51, 1813–1830, doi:10.1002/2014WR015696, 2015.

Reeves, J. M., Barrows, T. T., Cohen, T. J., Kiem, A. S., Bostock, H. C., Fitzsimmons, K. E., Jansen, J. D., Kemp, J., Krause, C., Petherick, L., and Phipps, S. J.: Climate variability over the last 35,000 years recorded in marine and terrestrial archives in the Australian region: an OZ-INTIMATE compilation, Quaternary Sci. Rev., 74, 21–34, doi:10.1016/j.quascirev.2013.01.001, 2013.

Risbey, J. S., Pook, M. J., McIntosh, P. C., Wheeler, M. C., and Hendon, H. H.: On the remote drivers of rainfall variability in Australia, Mon. Weather Rev., 137, 3233–3253, 2009.

Roberts, J., Plummer, C., Vance, T., van Ommen, T., Moy, A., Poynter, S., Treverrow, A., Curran, M., and George, S.: A 2000 year annual record of snow accumulation rates for Law Dome, East Antarctica, Clim. Past, 11, 697–707, doi:10.5194/cp-11-697-2015, 2015.

Sheppard, P. R., Tarasov, P. E., Graumlich, L. J., Heussner, K. U., Wagner, M., Österle, H., and Thompson, L. G.: Annual precipitation since 515 BC reconstructed from living and fossil juniper growth of northeastern Qinghai Province, China, Clim. Dynam., 23, 869–881, doi:10.1007/s00382-004-0473-2, 2004.

Speer, M. S.: On the late twentieth century decrease in Australian east coast rainfall extremes, Atmos. Sci. Lett., 9, 160–170, 2008.

Speer, M. S., Wiles, P., and Pepler, A.: Low pressure systems off the New South Wales coast and associated hazardous weather: establishment of a database, Austr. Meteorol. Oceanogr. J., 58, 29–39, 2009.

Timbal, B.: The climate of the Eastern Seaboard of Australia: a challenging entity now and for future projections, IOP Conference Series: Earth and Environmental Science, Canberra, Australia, 27–29 January 2010, 11, 012013, 2010.

Timbal, B. and Drosdowsky, W.: The relationship between the decline of Southeastern Australian rainfall and the strengthening of the subtropical ridge, Int. J. Climatol., 33, 1021–1034, doi:10.1002/joc.3492, 2013.

Tozer, C. R., Kiem, A. S., and Verdon-Kidd, D. C.: On the uncertainties associated with using gridded rainfall data as a proxy for observed, Hydrol. Earth Syst. Sci., 16, 1481–1499, doi:10.5194/hess-16-1481-2012, 2012.

Twomey, C. and Kiem, A. S.: East Coast Lows (ECLs) and rainfall along the eastern seaboard of Australia (ESA) – comparison of datasets used to record ECL occurrence and impacts on rainfall, Mon. Weather Rev., in review, 2015a.

Twomey, C. and Kiem, A. S.: Spatial and temporal inhomogeneity of rainfall patterns in Australia – Why is the eastern seaboard of Australian (ESA) different and why does inhomogeneity also exist within the ESA?, Int. J. Climatol., in review, 2015b.

HESSD

12, 12483–12514, 2015

van Ommen, T. D., and Morgan, V.: Snowfall increase in coastal East Antarctica linked with southwest Western Australian drought, Nature Geosci., 3, 267–272, doi:10.1038/ngeo761, 2010.

Vance, T. R., van Ommen, T. D., Curran, M. A. J., Plummer, C. T., and Moy, A. D.: A millennial proxy record of ENSO and Eastern Australian rainfall from the Law Dome ice core, East Antarctica, J. Climate, 26, 710–725, doi:10.1175/JCLI-D-12-00003.1, 2013.

Vance, T. R., Roberts, J. L., Plummer, C. T., Kiem, A. S., and van Ommen, T. D.: Interdecadal Pacific variability and eastern Australian megadroughts over the last millennium, Geophys. Res. Lett., 42, 129–137, doi:10.1002/2014GL062447, 2015.

Verdon, D. C. and Franks, S. W.: Indian Ocean sea surface temperature variability and winter rainfall: eastern Australia, Water Resour. Res., 41, W09413, doi:10.1029/2004wr003845, 2005.

Verdon, D. C. and Franks, S. W.: Long-term behaviour of ENSO: interactions with the PDO over the past 400 years inferred from paleoclimate records, Geophys. Res. Lett., 33, L06712, doi:10.1029/2005GL025052, 2006.

Verdon, D. C. and Franks, S. W.: Long-term drought risk assessment in the Lachlan River Valley – a paleoclimate perspective, Australian J. Water Resour., 11, 145–152, 2007.

Verdon, D. C., Wyatt, A. M., Kiem, A. S., and Franks, S. W.: Multidecadal variability of rainfall and streamflow: eastern Australia, Water Resour. Res., 40, W10201, doi:10.1029/2004wr003234, 2004.

Verdon-Kidd, D. C. and Kiem, A. S.: Nature and causes of protracted droughts in southeast Australia: comparison between the Federation, WWII, and Big Dry droughts, Geophys. Res. Lett., 36, L22707, doi:10.1029/2009gl041067, 2009.

Verdon-Kidd, D. C. and Kiem, A. S.: Quantifying Drought Risk in a Nonstationary Climate, J. Hydrometeorol., 11, 1019–1031, doi:10.1175/2010jhm1215.1, 2010.

Whan, K., Timbal, B., and Lindesay, J.: Linear and nonlinear statistical analysis of the impact of sub-tropical ridge intensity and position on south-east Australian rainfall, Int. J. Climatol., doi:10.1002/joc.3689, 2013.

HESSD

12, 12483–12514, 2015

An ice core derived 1013-year catchment scale annual rainfall reconstruction

C. R. Tozer et al.

Table 1. Pearson correlation values between LD_{SSS} and 12 month average (October–September) rainfall recorded at gauge 61010 and the AWAP WR catchment average for the 1900–2010 period and IPO phases. Bootstrap 95 % confidence intervals are also indicated (Mudelsee, 2003). Bold values are significant at 95 %.

Time Period	61010	AWAP catchment average
Full record (1900–2010)	**0.29** [0.12–0.45]	**0.28** [0.10–0.44]
IPO positive (1924–1941, 1979–1997)	**0.47** [0.23–0.66]	**0.55** [0.31–0.73]
IPO positive (1924–1941)	**0.33** [0.01–0.59]	0.34 [−0.11–0.68]
IPO positive (1979–1997)	**0.59** [0.23–0.81]	**0.67** [0.44–0.82]
IPO negative (1947–1975)	**0.37** [0.13–0.57]	**0.32** [0.06–0.54]

Table 2. Duration of longest dry and wet periods for the AWAP and reconstructed rainfall.

Mean (mm) used to determine wet/dry	SD (mm) used to determine wet/dry	x value used to determine wet/dry (Threshold = Mean $\pm x \times$ SD)	Duration of longest DRY period (years)	DRY period	Duration of longest WET period (years)	WET period
		AWAP catchment average rainfall (1900–2010)				
1100.0 (1900–2010)	264.6 (1900–2010)	0 (Mean)	8	1935–1942	5	1927–1931
		0.1	8	1935–1942	8	1925–1932
		0.2	8	1935–1942	8	1925–1932
		0.3	8	1935–1942	8	1925–1932
		0.4	8	1935–1942	9	1948–1956
		0.5	9	1979–1987	9	1924–1932, 1948–1956, 1971–1979
		Reconstructed Rainfall (1900–2010)				
1100.0 (1900–2010)	73.9 (1900–2010)	0 (Mean)	7	1936–1942	7	1907–1913
		0.1	7	1936–1942	8	1907–1914
		0.2	8	1935–1942	10	1905–1914
		0.3	8	1935–1942	10	1905–1914
		0.4	9	1973–1981	10	1905–1914
		0.5	11	1973–1983	10	1905–1914
		Reconstructed Rainfall (1000–2012)				
1100.0 (1900–2010)	73.9 (1900–2010)	0 (Mean)	7	1936–1942	16	1499–1605, 1834–1849
		0.1	9	1215–1223	26	1831–1856
		0.2	9	1215–1223	27	1830–1856
		0.3	12	1193–1204	39	1830–1868
		0.4	12	1193–1204	39	1830–1868
		0.5	12	1193–1204, 1212–1223	39	1830–1868
		Reconstructed Rainfall (1000–2012)				
1126.1 (1000–2012)	83.0 (1000–2012)	0 (Mean)	12	1193–1204	16	1834–1849
		0.1	12	1193–1204	16	1834–1849
		0.2	12	1193–1204	16	1834–1849
		0.3	17	1117–1133	16	1589–1605, 1834–1849
		0.4	17	1117–1133	26	1831–1856
		0.5	18	1206–1223	27	1830–1856

HESSD
12, 12483–12514, 2015

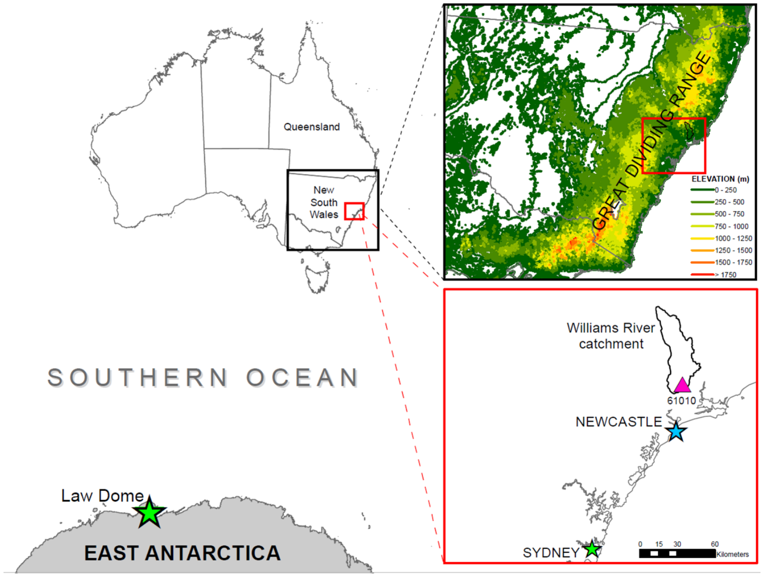

Figure 1. Location of Law Dome in relation to Australia with insets indicating the Great Dividing Range, WR catchment boundary and the location of 61010 high quality rainfall gauge, Newcastle and Sydney.

HESSD
12, 12483–12514, 2015

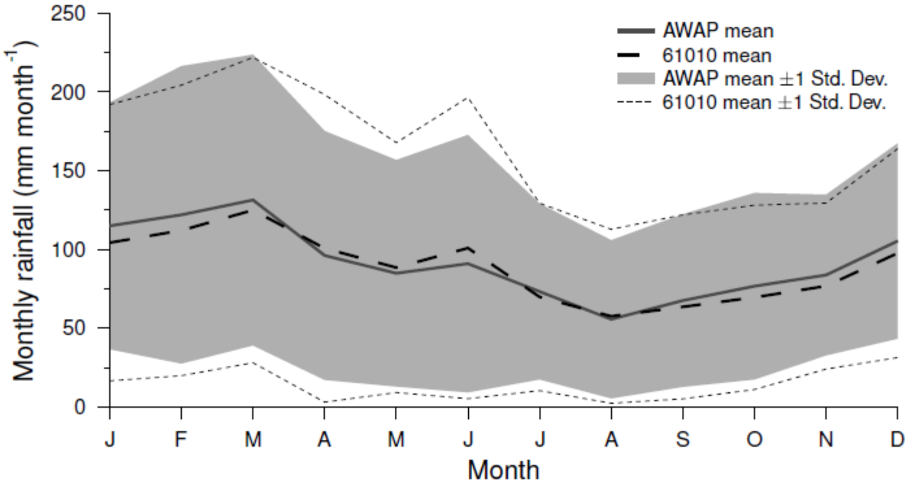

Figure 2. Annual climatology of WR catchment rainfall.

HESSD

12, 12483–12514, 2015

An ice core derived 1013-year catchment scale annual rainfall reconstruction

C. R. Tozer et al.

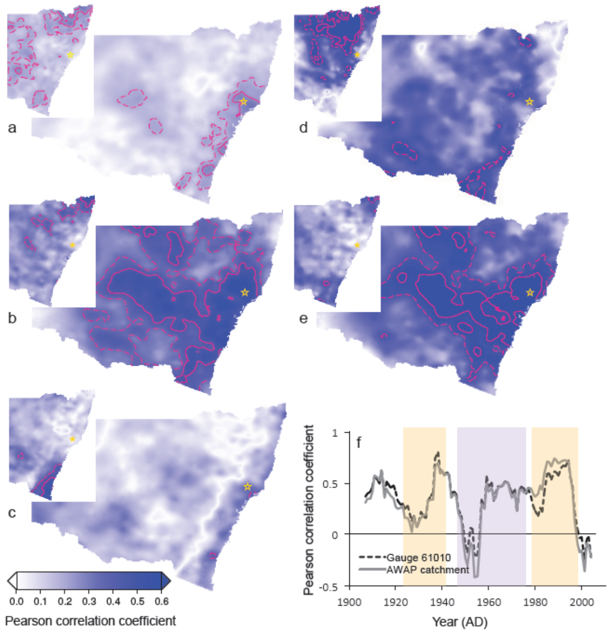

Figure 3. Correlations between **(a)** 12 month average (October–September) AWAP rainfall and LD_{SSS} for the 1900–2010 period with inset showing correlations between annual AWAP rainfall calculated from January–December and LD_{SSS} for 1900–2010 period, **(b)** as in **(a)** but for the combined IPO positive phases (1924–1941, 1979–1997), **(c)** as in **(a)** but for the IPO negative phase (1947–1975), **(d)** as in **(a)** but for the first IPO positive (1924–1941) phase **(e)** as in **(a)** but for the second IPO positive (1979–1997) phase and **(f)** 13 year moving window correlations between 12 month average (October–September) rainfall recorded at gauge 61010 and the AWAP WR catchment average and LD_{SSS} with shading indicating IPO positive (yellow) and IPO negative (purple) phases. Note that for **(a)–(e)** the star represents the location of the WR catchment centroid, dashed pink line shows 95 % significance level, bold pink line shows 99 % significance level.

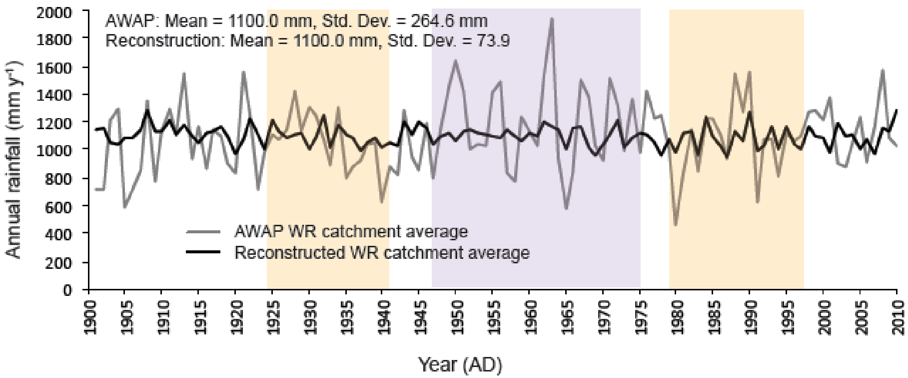

Figure 4. Reconstructed (black) and AWAP (grey) WR catchment average rainfall. Shading indicates IPO positive (yellow) and IPO negative (purple) phases.

HESSD
12, 12483–12514, 2015

An ice core derived 1013-year catchment scale annual rainfall reconstruction

C. R. Tozer et al.

Title Page
Abstract Introduction
Conclusions References
Tables Figures
◀◀ ▶▶
◀ ▶
Back Close
Full Screen / Esc
Printer-friendly Version
Interactive Discussion

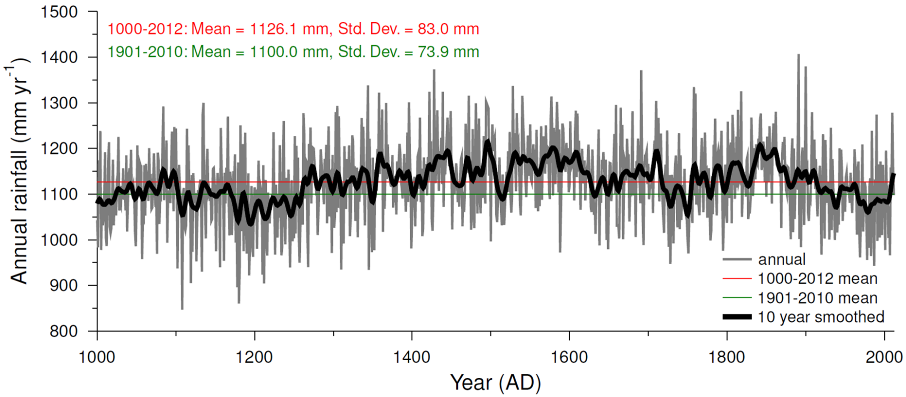

Figure 5. WR catchment rainfall reconstruction (grey line), 10 year Gaussian smooth (bold black line), mean of the rainfall reconstruction for 1000–2012 period (red line) and 1900–2010 period (green line).

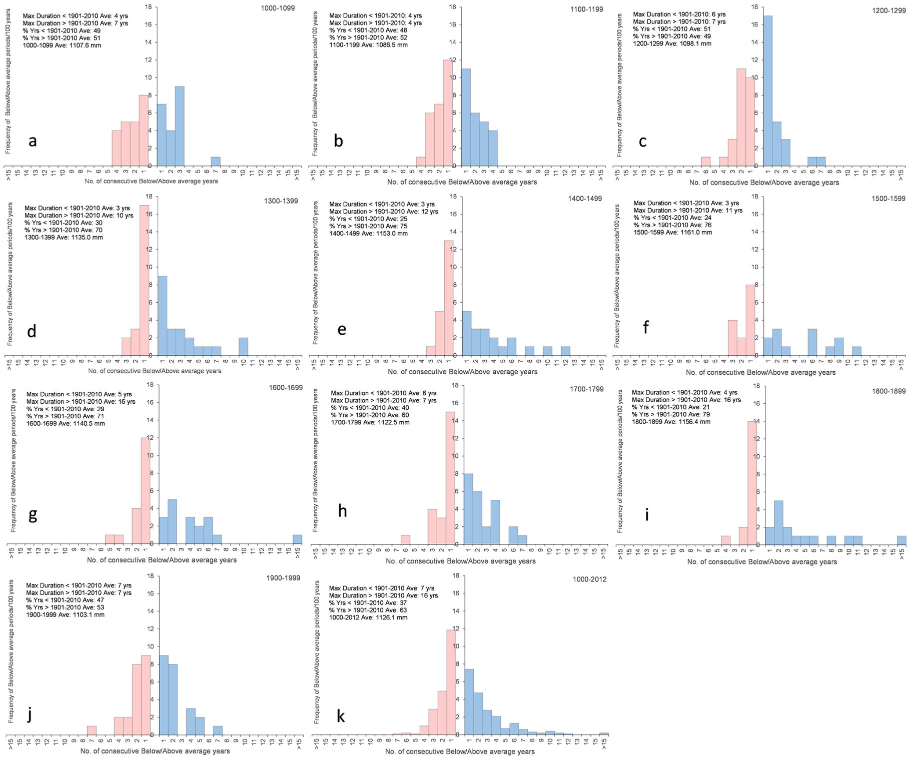

Figure 6. Histograms of duration of above (blue) and below (pink) average rainfall periods in each century since AD 1000. **(a–j)** Are centennial subsets and **(k)** is the AD 1000–2012 period (note different axis scaling). Above/below average are defined using $x = 0$ in Eq. (1) (as per Table 2).

HESSD
12, 12483–12514, 2015

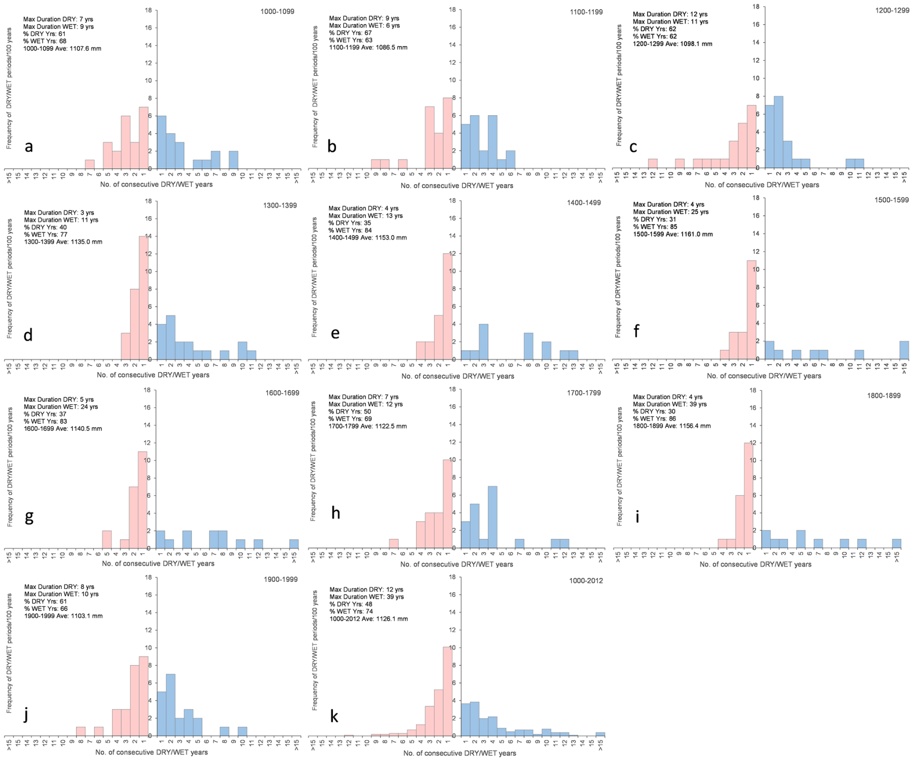

Figure 7. Histograms of duration of WET (blue) and DRY (pink) average periods during each century since AD 1000. **(a–j)** are centennial subsets and **(k)** is the AD 1000–2012 period (note different axis scaling). WET/DRY are defined using $x = 0.3$ in Eq. (1) (as per Table 2).

HESSD
12, 12483–12514, 2015

An ice core derived 1013-year catchment scale annual rainfall reconstruction

C. R. Tozer et al.